Competitive Interactions of NH$_3$ and Toluene with Biochar Modified by Pre- and Post-Treatments of H$_3$PO$_4$ in Dual Adsorption Systems

Mingxue Su, Ning Li,* Ting Huang, and Bing Zhu

Biochar modified by H$_3$PO$_4$ treatment can be used to purify malodorous gases during bio-drying of sludge, but the current understanding of multi-component adsorption of malodorous gases through biochar is limited. This study examined the adsorption mechanism of mixed malodorous gases including toluene and ammonia (NH$_3$) on two kinds of biochar modified *via* H$_3$PO$_4$ pretreatment before and after pyrolysis. The biochar obtained by H$_3$PO$_4$ pretreatment of biomass before pyrolysis (C550) preferred to adsorb NH$_3$ whether in the single or the dual system. In contrast, the biochar obtained by H$_3$PO$_4$ reprocessing after pyrolysis of biomass (C350-550) tended to adsorb toluene in the dual system but was more efficient in absorbing NH$_3$ in the single system. The pseudo-second-order kinetic model indicated the synergistic adsorption between NH$_3$ and toluene for all biochar samples. In-situ DRIFTS of C350-550 during adsorption demonstrated the formation of amino functional groups caused by NH$_3$ chemical adsorption with -OH (or -COOH) in the dual system. These increases in basic groups on C350-550 could enhance the surface zero potential point of C350-550, thereby improving the non-polarity of C350-550 and benefit the adsorption of weak polar toluene.

*Contact information: Hefei Cement Research and Design Institute Corporation Ltd, Hefei, 230022, Anhui, China; *Corresponding author: lining@hcrdi.com*

INTRODUCTION

Compared with thermal drying, sludge bio-drying is prospective due to the reduced energy consumption (Zheng *et al*. 2021; Zhao *et al*. 2022a). However, malodorous pollutants, such as gaseous ammonia (NH$_3$) and volatile organic compounds (VOCs), are considered to be a key problem restricting the development of sludge bio-drying (Maulini-Duran *et al*. 2013; Duan *et al*. 2022). An effective technology to remove colorless, corrosive, and harmful gas is thus necessary to protect human health from the serious pungent smell (González *et al*. 2019; Wang *et al*. 2022a).

Adsorption has been considered to be the most cost-effective method for removing NH$_3$ and toluene because of its mild operating conditions and product safety (Wysocka *et al*. 2019). Biochar, an environment-friendly adsorptive material, had been widely used to remove NH$_3$ and toluene because of its high surface areas, abundant surface functional groups and pore structures, and the potential utilization of various waste biomasses for production (Zhang *et al*. 2017; Kim *et al*. 2020; Cha *et al*. 2022; Seo *et al*. 2022; Cho *et al*. 2023). More attention has been paid to the modification or activation of biochar to further improve the adsorption ability of NH$_3$ and toluene. Compared with other chemical

activation methods such as sulfuric acid (H_2SO_4), potassium hydroxide (KOH), and zinc chloride ($ZnCl_2$), phosphoric acid (H_3PO_4) treatment showed unique advantages such as relatively mild pyrolysis conditions, low corrosivity to the equipment, minor pollution, and low costs (Yue *et al*. 2021; Zhu *et al*. 2022). In particular, oxygen functional groups, which greatly benefit the adsorption of NH_3 and toluene, could be introduced into biochar by H_3PO_4 treatment (Cao *et al*. 2018; Chu *et al*. 2018; Liu *et al*. 2019). Fernandez *et al*. (2015) investigated the characteristics of biochar after H_3PO_4 post-treatment and observed more developed porosity of biochar for the adsorption of emerging organic pollutants. Liu *et al*. (2019) compared the removal ability of biochar treated by KOH and H_3PO_4 to methylene blue in wastewater and indicated that the adsorption capacity of biochar had been increased by five times as a consequence of the electrostatic interaction between the aromatic ring structure of biochar and phosphorus-containing functional groups. Chu *et al*. (2018) investigated the effect of H_3PO_4 treatment on the development of the porous structure of biochar and found a well-developed microporous structure and high specific surface area. These attributes were attributed to the catalytic effect of hydrogen protons provided by H_3PO_4 and the crosslink of cellulose structure with acid.

However, most of the present works focused on the adsorptive removal ability of biochar in a single system, or in a dual system consisting of the same type of contaminant gases like ethylbenzene, acetone, and toluene (Zhang *et al*. 2017; Jayawardhana *et al*. 2021; Rajabi *et al*. 2021). The malodorous gases produced by sludge bio-drying were mixed gases simultaneously containing inorganic and organic gases, such as NH_3 and VOCs (Chen *et al*. 2021, 2022; Zeng *et al*. 2022; Zhao *et al*. 2022b). Therefore, the effects of pre-carbonization before H_3PO_4 treatment on the pore structure and surface functional groups of biochar need to be studied. In addition, the dynamic changes in the physicochemical properties of biochar caused by chemical adsorption and the competitive interactions between inorganic and organic gases on biochar surfaces during adsorption process need to be also investigated.

Herein, two kinds of biochar were prepared by H_3PO_4 treatments: one was produced by H_3PO_4 pretreatment of biomass before pyrolysis, and the other was obtained by H_3PO_4 reprocessing after pre-pyrolysis of biomass. The effects of H_3PO_4 treatments on the changes in the characteristics of final biochar production were systematically explored. Most importantly, the competitive interaction mechanism between organic and inorganic malodorous gases on biochar surface as well as the resulting changes in physicochemical properties and adsorption behaviors of biochar were explained in-depth.

EXPERIMENTAL

Materials

Rice husk (RH), obtained from local farmland (Hefei, Anhui, China), was utilized to produce biochar. RH was ground to pass through a 20-mesh sieve. The obtained powder was washed by DIW and dried at 80 °C for 3 days. Phosphoric acid (H_3PO_4, AR, 85%), sodium hydroxide (NaOH, AR, 96%), and toluene were purchased from Sigma-Aldrich, Inc. (Shanghai, China). Ammonia standard gas (NH_3) was provided by Xuancheng Source Gas Industry Co., Ltd. (Anhui, China). All reagents were used as received.

Biochar Preparation

As the suitable pyrolysis temperature for the preparation of biochar by H_3PO_4 modification was set to be 550 °C (Sun *et al*. 2018; Wang *et al*. 2022b; Cao *et al*. 2018), the final pyrolysis temperature of all biochar productions after H_3PO_4 treatment was unified at this temperature. The difference among these biochar samples was whether the pre-pyrolysis process was carried out in the preparation process.

In a typical preparation, RH powder was directly immersed into a 2 M H_3PO_4 solution, and the ratio of powder to H_3PO_4 solution was 1:10 (g powder: mL solution). After stirring and drying, the mixture was pyrolyzed at 550 °C for 1 h under a nitrogen atmosphere to obtain the biochar. This production was washed by DIW until the filtrate was neutral. Finally, this production was labeled as C550.

In comparison, RH powder was first placed into a tube furnace and treated at 350 °C, 550 °C, and 750 °C for 30 min under a nitrogen atmosphere, respectively. After pyrolysis, the obtained powder was immersed into a 2 M H_3PO_4 solution, followed by stirring for 1 h and drying at 80 °C overnight. The ratio of powder to H_3PO_4 solution was 1:10 (g powder: mL solution). The mixture was pyrolyzed at 550 °C for 1 h under a nitrogen atmosphere to obtain the biochar. These productions were labeled as C350-550, C550-550, and C750-550, respectively.

For ease of description, the process of producing C350-550, C550-550, and C750-550 was defined and simplified as the H_3PO_4 post-treatment method with pre-carbonization. Similarly, the process of producing C550 was defined and simplified as the H_3PO_4 pre-treatment method.

Biochar Characterization

The textural properties of biochar were obtained using an Autosorb iQ (Quantachome, USA). Fourier transform infrared spectroscopy (FTIR) of biochar was detected by Nicolet IS200 (ThermoFisher, USA) using KBr disks. The elemental compositions of biochar were measured using an elemental analyzer (Vario EL III, German). Raman spectroscopy of biochar was determined by LabRAM Soleil (HORIBA, Japan). *In situ* diffuse reflectance Fourier transform infrared spectroscopy (In-situ DRIFTS) system, including Nicolet iS50 Vertical leaf infrared spectrometer, MCT detector (Negoli, USA), Harrick *in situ* diffuse reflection accessory (ZnSe window sheet), and self-made gas circuit control system was used to detect the changes of surface functional groups during the adsorption process of biochar for NH_3 and toluene. The pH of biochar was measured by SevenDirect SD20 HA Kit (Mettler Toledo, USA) following the guidance from the previous literature (Liu *et al*. 2021).

Adsorption Experiments

The adsorption experiments were performed at room temperature under atmospheric pressure on a self-built experimental device (Scheme S1). For the binary system, firstly, a certain mass of the sample was fixed into a quartz tube. The inner diameter of the quartz tube was 10 mm and the length of the sample in the quartz tube was maintained at 108 mm. Sequentially, the sample was activated with pure N_2 at 150 °C for 2 h under a gas flow rate of 50 standard cubic centimeter per minute (sccm). After cooling, a gas mixture containing 500 ppm NH_3, 500 ppm toluene, and the balance N_2 was introduced into the quartz tube to start the evaluation of adsorption performance with the gas flow rate of 500 sccm. The outlet concentration of the gas mixture was monitored by Gas Chromatography and Mass Spectrometry (GC-MS, Shimadzu, QP2020NX, Japan).

For the single system, the methodology was the same as that of the binary system except for the gas mixture only containing 500 ppm NH_3 or toluene and the balance N_2.

The adsorption breakthrough curve was determined by the plot of C_t/C_0 versus time and was also utilized to calculate the adsorption capacity of NH_3 or toluene of biochar. The formula was defined as follows (Cheng *et al*. 2020),

$$Q = q_{in} \times C_{n0} \times \Delta t - \int_0^t q_{out} C_{nt} dt \qquad (1)$$

where Q is adsorption capacity (mL), q_{in} is the inlet flow rate of the gas mixture (mL/min), q_{out} is the outlet flow rate of the gas mixture (mL/min), C_{n0} is the inlet concentration of toluene or NH_3 (%), C_{nt} is the outlet concentration of toluene or NH_3 at a certain time (%), t is defined as the adsorption duration (s), and Δt is defined as the total adsorption time (s).

RESULTS AND DISCUSSION

Biochar Properties

The textural properties of all biochar samples are summarized in Table 1. The BET surface area and total pore volume of C550 were 284 m^2/g and 0.769 mL/g, which was higher than 181 m^2/g and 0.133 mL/g of C350-550, 263 m^2/g and 0.196 mL/g of C550-550, and 94.8 m^2/g and 0.102 mL/g of C750-550, respectively. However, the micropore volume of C550 was only 0.0278 mL/g, which was lower than 0.0743 mL/g of C350-550, 0.0921 mL/g of C550-550, and 0.0281 mL/g of C750-550, respectively. The comparison results indicated that the textural properties of biochar were significantly affected by different H_3PO_4 treatment methods. The surface area and total pore volume can be improved by the H_3PO_4 pre-treatment method, while the micropore volume can be enhanced *via* the H_3PO_4 post-treatment method. Another observation was that the average pore size of C350-550, C550-550, and C750-550 was about 2 to 4 nm, which was significantly smaller than that of about 10 nm of C550.

Table 1. The Textural Properties of All Biochar Samples

Samples	[a]S_{BET}(m^2/g)	[b]V_{total}(mL/g)	[c]V_{micro}(mL/g)	Average pore size(nm)
C550	284	0.769	0.0208	10.85
C350-550	181	0.133	0.0743	2.93
C550-550	263	0.196	0.092	2.99
C750-550	270	0.198	0.952	4.81

[a]Determined by N_2 adsorption–desorption isotherms at 77 K
[b]Determined by the amount adsorbed at $P/P_0 = 0.99$
[c]Determined by the t-plot method

The improvement of textural properties by H_3PO_4 treatment was ascribed to the chemical reactions between H_3PO_4 and raw biomass or biochar. Because H_3PO_4 is an acid catalyst, it can enhance the bond cleavage and crosslink reaction (Chu *et al*. 2018). The intramolecular or intermolecular dehydration of the biopolymer in biomass was accelerated under the catalysis of polyphosphoric acid by the dehydration of H_3PO_4 during the carbonization process, which produced a large amount of gases and steam. On the other hand, the C-O bond of alcohol or ether groups in biochar was attacked by hydrogen protons released from H_3PO_4, followed by lots of gases and steam forming and releasing during the pyrolysis process. These generated gases contributed to the high specific surface area

and large pore volume. It was worth noting that mesopores were dominant for C550, but the micropores were governing for C350-550, C550-550, and C750-550. This phenomenon was owing to two main reasons: the decomposition of crystalline cellulose in biomass was serious in the presence of H_3PO_4 during the pyrolysis, resulting in the fragmentation of carbon skeleton structure and the generation of more mesopore rather than micropore. Meanwhile, the pre-pyrolysis for producing biochar such as C350-550 decomposed a large number of organic fractions, and the crosslink reaction between the rigid carbon skeleton structure of C350-550 and H_3PO_4 was limited and generated micropores.

Two spectral peaks with Raman shifts of 1350 cm^{-1} (D-band) and 1590 cm^{-1} (G-band) were distinctly observed in all biochar samples (Fig. 1), which corresponded to the disordered carbon structures and in-plane graphite vibrations, respectively. The ratio of the area of the D-band (AD) to the area of the G-band (AG) was applied to evaluate the integral heterogeneity in the C structure of biochar samples obtained by different H_3PO_4 treatment methods (Chen *et al*. 2021). The ratio of AD/AG was 1.70 for C550, 1.66 for C350-550, 1.63 for C550-550, and 1.66 for C750-550, respectively. These results revealed that the H_3PO_4 pre-treatment method could increase the disorder degree of the final biochar. In addition, compared with the biochar obtained from the H_3PO_4 post-treatment method, the fragmentation of carbon skeleton structure was generated intensely with the pyrolysis of biomass and H_3PO_4, in terms of with the H_3PO_4 pre-treatment method (C550).
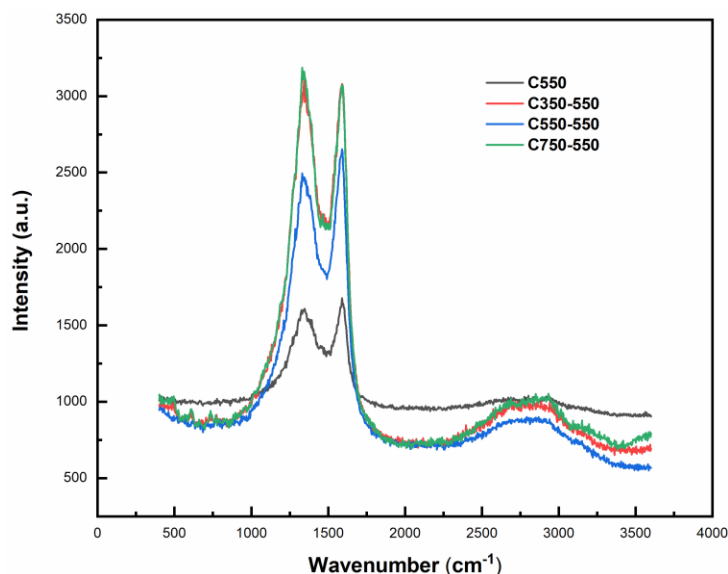
Fig. 1. Raman spectra of all biochar samples. Test conditions: 532 nm laser, 50 times objective lens, 10 mW power, 5 s acquisition time, 2 cycles

The FTIR spectra are presented in Fig. 2. The functional groups of all biochar samples are displayed in Table 2. The main functional groups included Si-O-Si, aromatic ring or substituted aromatic ring, carboxyl, C=O and C=C, aliphatic C, and hydroxyl. In particular, the characteristic peaks of 1147 cm^{-1} indicated the presence of aminophosphonic acid functional groups. The characteristic peaks of 1170 cm^{-1} corresponded to the stretching vibration of the P-O (hydrogen-bonded) bond, to the O=P-OH bond, or to the O–C stretching vibration of the P-O-C bond, revealing the presence of phosphorus or phosphocarbonaceous compounds. These results implied that H_3PO_4 reacted with the carbon of biomass or biochar during the pyrolysis process, and a part of phosphorous existed in the form of functional groups on the surface of the final biochar. The intensity

of 1147 cm^{-1} and 1170 cm^{-1} of C350-550, C550-550, and C750-550 absorbances were stronger than C550, indicating that the phosphorus functional group was easier to form by the H$_3$PO$_4$ post-treatment method. For C350-550, there was a distinct characteristic peak at 990 cm^{-1}, which corresponded to the P-OH group (Shen and Zhang 2019).
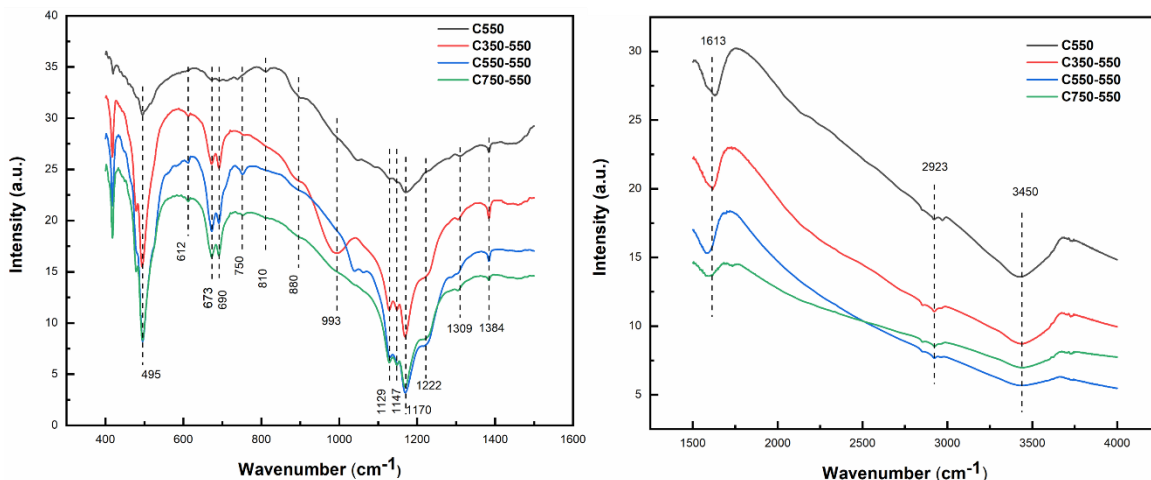
Fig. 2. FTIR spectra of all biochar samples under the wavenumber ranging from 400 to 1500 cm^{-1} (left) and from 1500 to 4000 cm^{-1} (right)

Table 2. The Exhaustive Functional Groups of All Biochar Samples

Wavenumber (cm^{-1})	Main Functional Groups	References
495	Si-O-Si	Liu *et al.* 2019
993	P-OH	Shen and Zhang 2019
673, 690, 750, 810, 880	aromatic ring or substituted aromatic ring	Barroso-Bogeat *et al.* 2015
1147	aminophosphonic acid	Liu *et al*. 2019
1170	the stretching vibration of P-O (hydrogen-bonded) bond, O=P-OH, the O–C stretching vibration of the P-O-C bond	Cordero-Lanzac *et al.* 2017
1384	Carboxyl and bending vibration of -OH	Liu *et al.* 2019
1613	C=O and C=C	Liu *et al.* 2019
2923	aliphatic C	Cao *et al.* 2018
3450	-OH	Liu *et al.* 2019

The elemental analysis (C, H, and O) of all biochar samples is summarized in Table 3. The C content of C350-550, C550-550, and C750-550 increased with the increase of pre-pyrolysis temperature, while the O content of these samples appeared the opposite tendency. In addition, the C and O content of C350-550, C550-550, and C750-550 were higher than C550, suggesting that the H$_3$PO$_4$ post-treatment method was beneficial to the retention of carbon skeleton and oxygen content compared with the H$_3$PO$_4$ pre-treatment method. The H/C and O/C atomic ratios were applied to evaluate the aromaticity and polarity of biochar samples, respectively. The ratio of H/C was 0.043 for C350-550, 0.037 for C550-550, and 0.043 for C750-550, which was higher than 0.036 for C550, indicating that more aromatic structures were present in C350-550, C550-550, and C750-550. Thus, the pre-carbonization was favorable to forming aromatic structures and retaining aromatic

structures during subsequent H_3PO_4 treatment (Chu *et al*. 2018). The ratio of O/C for C350-550, C550-550, and C550 showed the same trend as the ratio of H/C. Combined with the FTIR spectra, it could be inferred that the surface of biochar had more intensified phosphorus oxygen species by the H_3PO_4 post-treatment method than by the H_3PO_4 pre-treatment method.

Table 3. The Elemental Analysis (C, H, and O) of All Biochar Samples

Samples	C	H	O	H/C	O/C
C550	70.17	2.59	22.15	0.036	0.32
C350-550	73.42	3.14	25.95	0.043	0.35
C550-550	73.81	2.75	25.41	0.037	0.34
C750-550	74.61	3.23	23.15	0.043	0.31

Performance and Mechanism of Biochar Adsorption to NH_3 And Toluene

To investigate the adsorption behavior of NH_3 and toluene in the dual system, the dynamic adsorption experiments of all biochar samples were conducted. The adsorption breakthrough curve of NH_3 and toluene for all biochar samples are displayed in Fig.3. The duration corresponding to $C_t/C_0=0.05$ was defined as the breakthrough time, and the duration corresponding to $C_t/C_0=0.95$ was defined as the saturated adsorption time. For NH_3 adsorption, the breakthrough time was 9975.5 s/g for C550, 2930.1 s/g for C350-550, 6015.7 s/g for C550-550, and 354.2 s/g for C750-550, but for toluene adsorption, the breakthrough time was 5119.8 s/g for C550, 15524.1 s/g for C350-550, 4946.9 s/g for C550-550, and 91.5 s/g for C750-550, respectively. Among them, C550 had the largest specific surface area and could provide the most adsorption sites for NH_3 adsorption, which leads to a longer breakthrough time. For toluene, C350-550 has the most acidic oxygenated functional groups, and these functional groups could react with NH_3 during adsorption in the dual system, which leads to the formation of amino functional groups on the biochar (Fig.6). These amino functional groups could be turned into new adsorption sites to delay the critical time point of toluene, leading to the prolonging of the breakthrough time of toluene (Fig.7).
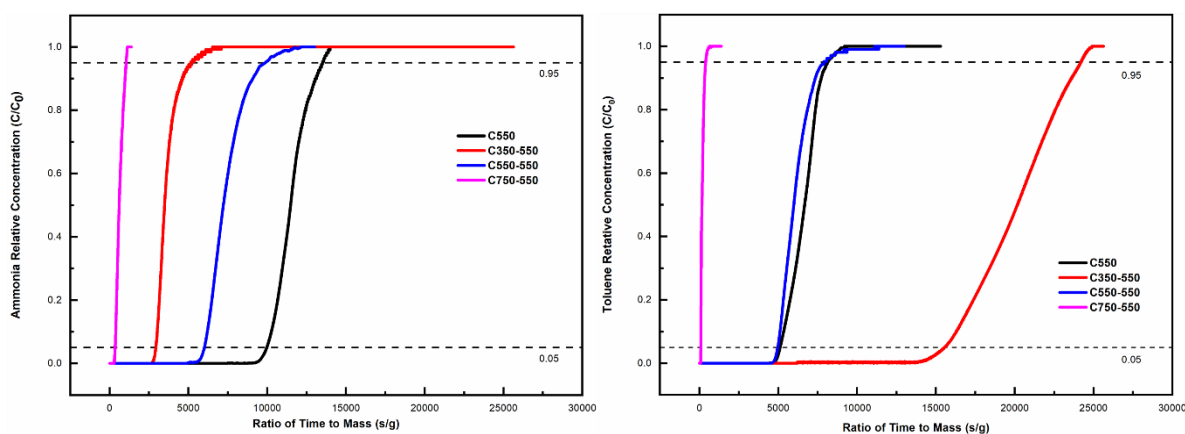

Fig. 3. The adsorption breakthrough curve of NH_3 (left) and toluene (right) for all biochar samples in the dual system

The saturated adsorption capacity for NH_3 and toluene of all biochar samples were present in Fig. 4. C550 possessed the highest NH_3 adsorption capacity, 38.5 mL/g, while

bioresources.com

C350-550 possessed the highest toluene adsorption capacity, 66.9 mL/g. C350-550 also had the highest total adsorption capacity of NH_3 and toluene, 79.2 mL/g. However, either NH_3 or toluene adsorption capacity was the lowest for C750-550, only 2.16 mL/g for NH_3 and 0.642 mL/g for toluene, respectively. In particular, C550 and C550-550 possessed similar toluene adsorption capacities, which corresponded to the adsorption breakthrough curve. According to these results, a conclusion could be drawn that H_3PO_4 pretreatment of biomass before pyrolysis was beneficial to NH_3 adsorption but H_3PO_4 reprocessing after pre-pyrolysis of biomass under 300 °C was preferred to toluene adsorption in the dual system.

The adsorption kinetics fitting results of the experimental data could provide a valuable reference for further analysis of the mechanism of the adsorption reaction. Therefore, the pseudo-first-order kinetic model and the pseudo-second-order kinetic model were applied (Hameed *et al*. 2007). The fitting results are shown in Tables S2 and S3. It can be seen that the fluctuation range of the R-square of the pseudo-first-order kinetic model (0.7414 to 0.9481 for NH_3 and 0.7113 to 0.9741 for toluene, respectively) was obviously wider than that of the pseudo-second-order kinetic model (0.9632 to 0.9998 for NH_3 and 0.9962 to 0.9999 for toluene, respectively). This suggests that biochar adsorption for NH_3 and toluene mixtures was controlled by a process of diffusion of adsorbate into a network of small pores (Hubbe *et al.* 2019).
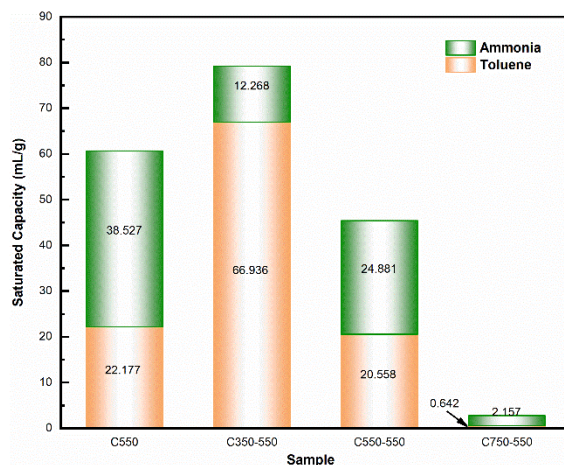
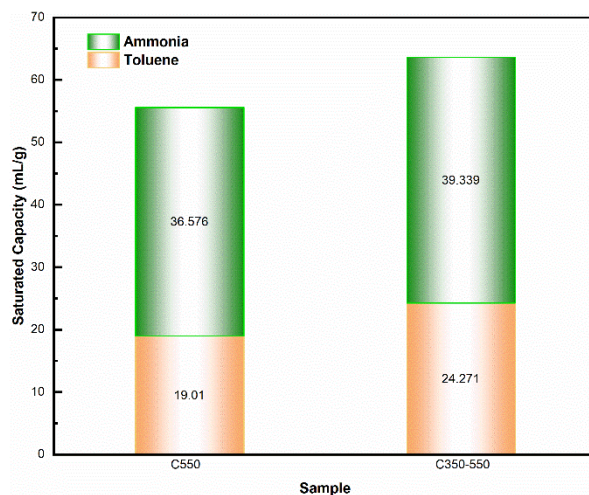**Fig. 4.** The saturated capacity of NH_3 and toluene for all biochar samples in the dual system

The adsorption mechanisms of biochar are explained by physical interaction, electrostatic interaction, the London dispersion component of van der Waals forces, π–π stacking, and hydrogen bonding. The dominant adsorption mechanisms were mainly decided by biochar physicochemical properties. Figure 5 shows that the C350-550 possessed the highest NH_3 adsorption capacity, corresponding to the largest micropore volume (Table 1) and the highest acidic O-containing functional group contents on the surface (Fig. 2). The large micropore volume could improve the adsorption capacity because most of the adsorbate was stored in the pores through micropore filling, and the high acidic O-containing functional group contents on the surface could also improve the adsorption capacity through acid-base interaction with the basic molecule of NH_3. Therefore, physical (micropore filling) and chemical interactions (acid-base interaction) were suggested to be the dominant NH_3 adsorption mechanisms (Zhang *et al*. 2022). For toluene, according to the previous literature (Feng *et al.* 2021), the N-containing functional

group can promote the adsorption of phenyl compound due to the change in the electrostatic potential on the surface of the biochar, which causes the deviation of the phenyl compound adsorption site and increases the van der Waals interaction between the two molecules. The result of *in-situ* DRIFTS in the present study shows the formation of a large amount of amine-containing functional groups during NH_3 adsorption, which is consistent with preconditions of Feng's study (Fig. 6). Therefore, van der Waals force adsorption was the main adsorption mechanism. In addition, the hydroxyl group as an electron donating group can enhance the interaction between electron clouds, thereby strengthening the π-π interaction. The FTIR results in this study showed the presence of -OH in the biochar samples. Thus, the pi-pi interaction was a supplementary mechanism.

The Effects of H_3PO_4 Treatment on Adsorption Mechanism of Biochar

According to the results in Fig. 4, C550 and C350-550 were selected as the typical samples to illustrate the effects of different H_3PO_4 treatments on the adsorption selectivity of NH_3 and toluene of biochar in the dual system in-depth. As shown in Fig. 5, the adsorptive performance of C550 in the single system was similar to that in the dual system. The adsorption capacity ratio of NH_3 to toluene in the single system was 1.92, which meant that C550 was still preferred to adsorb NH_3 in the single system. However, for C350-550, the adsorption selectivity between NH_3 and toluene in the single system was significantly different from that in the dual system. In the single system, the adsorption capacity of NH_3 was 39.3 mL/g, much higher than that of 12.3 mL/g in the dual system, and the adsorption capacity ratio of NH_3 to toluene in the single system was 1.62. This result indicated that C350-550 was also preferred to adsorb NH_3 in the single system, which was the same as C550.


Fig. 5. The saturated capacity of C550 and C350-550 for NH_3 and toluene in the single system

Combined with the kinetics results, an inference could be drawn that the chemical adsorption of NH_3 (or toluene) would cause dynamic changes in the physicochemical properties of biochar, leading to further enhancing (or weakening) adsorption behavior of toluene (or NH_3) in the dual system. The amine-containing sites were formed during the interactions between NH_3 molecules and –OH (or –COOH), introducing the basic N-containing groups such as pyridinic N and pyrrolic N (Wang *et al*. 2021) into the biochar samples. These increases in basic groups on the biochar surface could increase the surface zero potential point of the biochar, thereby increasing the non-polarity of the biochar and

benefiting the adsorption of weak polar toluene. As shown in Fig. 2, a large amount of P–OH and –COOH were present on the surface of C350-550, suggesting that more basic N-containing groups were formed and consequently the non-polarity of C350-550 was stronger than that of C550 during adsorption process in the dual system. Therefore, the toluene adsorption capacity of C350-550 in the dual system was much higher than that in the single system.

To further demonstrate this inference, the changes in functional groups of C350-550 during adsorption in the dual system were detected by In-Situ DRIFTS. As shown in Fig.6, the intensity of peak of 1500 to 1700 cm^{-1} increased with the adsorption of toluene. The peaks of 3048, 2829, and 993 cm^{-1} were considered as amino functional groups (Wang *et al*. 2021), and these peaks increased initially but remained unchanged later. In addition, the adsorption rate in the breakthrough curve of C350-550 was calculated. The time point at which the adsorption rate of NH$_3$ decreased in the dual system was earlier than that in the single system (Fig. 7). In contrast, the time point at which the adsorption rate of toluene decreased in the dual system was delayed compared with that in the single system. Furthermore, the spent C350-550 after NH$_3$ adsorption was reused to adsorb toluene in the single system, and the toluene capacity was 28.2 mL/g, higher than 24.3 mL/g of fresh C350-550 (Fig. 8). Besides, the adsorption capacity ratio of NH$_3$ to toluene decreased from 1.92 in the single system to 1.62 in the dual system, indirectly indicating the reasons for the phenomenon. Therefore, these experimental results were consistent with the above inference, demonstrating the formation of amino functional groups on the biochar caused by NH$_3$ adsorption in the dual system. These amino functional groups could be turned into new adsorption sites to delay the critical time point of toluene, leading to the increase of the adsorption capacity of toluene.
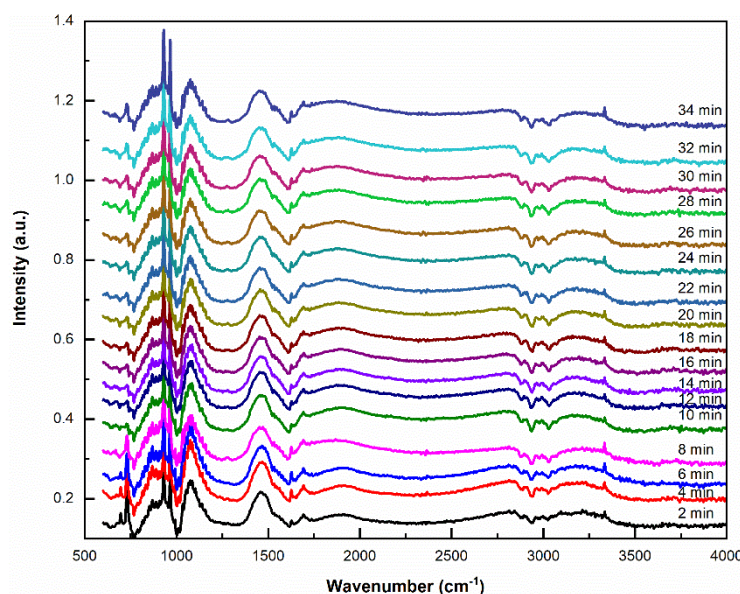
Fig. 6. *In-Situ* FTIR spectra of C350-550 during adsorption in the dual system
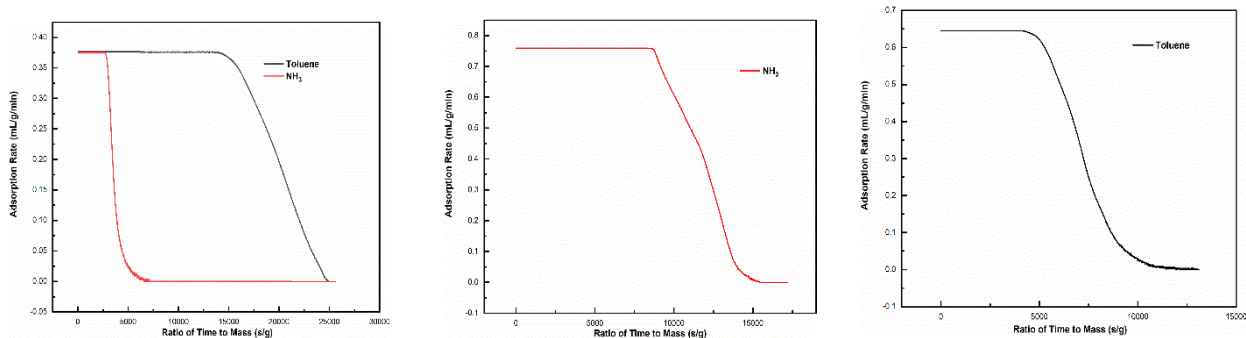
Fig. 7. The adsorption rate in the breakthrough curve of C350-550 for NH_3 and toluene in the dual system (left), NH_3 in the single system (middle), and toluene in the single system (right)
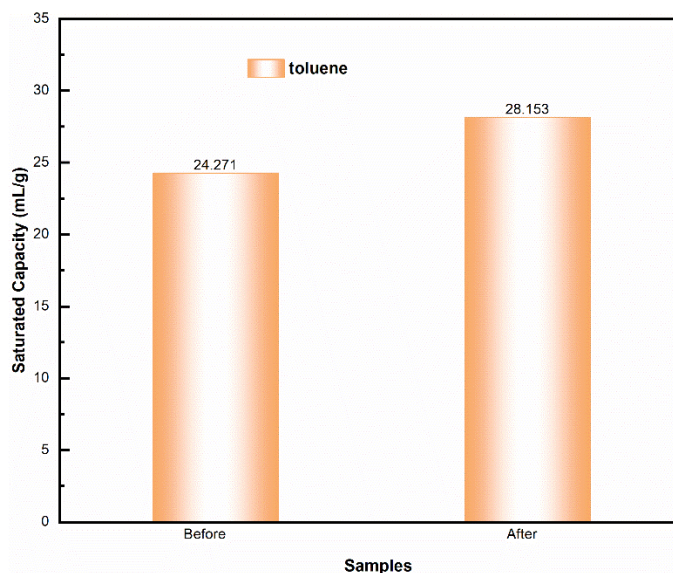
Fig. 8. The toluene capacity of C350-550 before and after NH_3 adsorption

CONCLUSIONS

1. Organic and inorganic volatile compounds exhibited competitive interactions on biochar surfaces modified by H_3PO_4 treatment during the adsorption process. These competitive interactions led to dynamic changes in the physicochemical properties of biochar, resulting in different adsorption behaviors.

2. In the dual system, different adsorption selectivity was observed among biochar samples: the biochar obtained by H_3PO_4 pretreatment of biomass before pyrolysis tended to adsorb NH_3, while the biochar obtained by H_3PO_4 reprocessing after pre-pyrolysis of biomass under low temperatures preferred to remove toluene.

3. Abundant surface acidic O-containing functional groups were introduced into biochar by post-treatment of H_3PO_4 under low temperatures. The enhanced non-polarity of biochar caused by the interactions between NH_3 molecules and these surface acidic O-containing functional groups during the adsorption process was considered to be the main reason for adsorptive selectivity.

bioresources.com

ACKNOWLEDGEMENTS

Competing Interests

The authors have no conflicts of interest to disclose, financial or otherwise.

Author Contributions

All authors contributed to the study conception and design. Material preparation, data collection and analysis were performed by Mingxue Su and Ting Huang. The first draft of the manuscript was written by Mingxue Su. The editing and improvement of manuscript were performed by Ning Li and Bing Zhu. All authors read and approved the final manuscript.

REFERENCES CITED

Barroso-Bogeat, A., Alexandre-Franco, M., Fernández-González, C., Macías-García, A., and Gómez-Serrano, V. (2015). "Temperature dependence of the electrical conductivity of activated carbons prepared from vine shoots by physical and chemical activation methods," *Micropor Mesopor Mat*. 209, 90-98. DOI: 10.1016/j.micromeso.2014.07.023

Cao, L. C., Yu, I. K. M., Tsang, D. C. W., Zhang, S. C., Ok, Y. S., Kwon, E. E., Song, H. C., and Poon, C. S. (2018). "Phosphoric acid-activated wood biochar for catalytic conversion of starch-rich food waste into glucose and 5-hydroxymethylfurfural," *Bioresource Technol.* 267, 242-248. DOI: 10.1016/j.biortech.2018.07.048

Cha, J. S., Kim, Y. M., Lee, I. H., Choi, Y. J., Rhee, G. H., Song, H., Jeon, B. H., Lam, S. S., Khan, M. A., Lin, K. Y. A., Chen, W. H., and Park, Y. K. (2022). "Mitigation of hazardous toluene *via* ozone-catalyzed oxidation using MnOx/Sawdust biochar catalyst," *Environ Pollut*. 312, 119920-119929. DOI: 10.1016/j.envpol.2022.119920

Chen, L., Li, W. G., Zhao, Y., Zhou, Y. J., Zhang, S. M., and Meng, L. Q. (2022). "Effects of compound bacterial agent on gaseous emissions and compost maturity during sewage sludge composting," *J. Clean Prod.* 366, 133015-133024. DOI: 10.1016/j.jclepro.2022.133015

Chen, Y. J., Syed-Hassan, S. S. A., Xiong, Z., Li, Q. L., Hu, X., Xu, J., Ren, Q. Q., Deng, Z. T., Wang, X. P., Su, S., Hu, S., Wang, Y., and Xiang, J. (2021). "Temporal and spatial evolution of biochar chemical structure during biomass pellet pyrolysis from the insights of micro-Raman spectroscopy," *Fuel Process. Technol*. 218, 106839-106846. DOI: 10.1016/j.fuproc.2021.106839

Cheng, H., Sun, Y. H., Wang, X. H., Zou, S. B., Ye, G. Z., Huang, H. M., and Ye, D. Q. (2020). "Hierarchical porous carbon fabricated from cellulose-degrading fungus modified rice husks: Ultrahigh surface area and impressive improvement in toluene adsorption," *J. Hazard. Mater*. 392, 122298-122305. DOI: 10.1016/j.jhazmat.2020.122298

Cho, S. H., Lee, S., Kim, Y., Song, H., Lee, J., Tsang, Y. F., Chen, W. H., Park, Y. K., Lee, D. J., Jung, S., and Kwon, E. E. (2023). "Applications of agricultural residue biochars to removal of toxic gases emitted from chemical plants: A review," *Sci. Total Environ*. 868, 161655-161674. DOI: 10.1016/j.scitotenv.2023.161655

Cordero-Lanzac, T., Hita, I., Veloso, A., Arandes, J.M., Rodríguez-Mirasol, J., Bilbao, J., Cordero, T., and Castaño, P. (2017). "Characterization and controlled combustion of carbonaceous deactivating species deposited on an activated carbon-based catalyst," *Chem. Eng. J*. 327, 454-464. DOI: 10.1016/j.cej.2017.06.077

Chu, G., Zhao, J., Huang, Y., Zhou, D. D., Liu, Y., Wu, M., Peng, H. B., Zhao, Q., Pan, B., and Steinberg, C. E. W. (2018). "Phosphoric acid pretreatment enhances the specific surface areas of biochars by generation of micropores," *Environ. Pollut*. 240, 1-9. DOI: 10.1016/j.envpol.2018.04.003

Duan, Z. H., Lu, W. J., Mustafa, M. F., Du, J. W., and Wen, Y. (2022). "Odorous gas emissions from sewage sludge composting windrows affected by the turning operation and associated health risks," *Sci. Total Environ*. 839, 155996-156004. DOI: 10.1016/j.scitotenv.2022.155996

Feng, D. D., Guo, D. W., Zhang, Y., Sun, S. Z., Zhao, Y. J., Shang, Q., Sun, H. L., Wu, J. Q., and Tan, H. P. (2021). "Functionalized construction of biochar with hierarchical pore structures and surface O-/N-containing groups for phenol adsorption," *Chem. Eng. J*. 410, 127707-127718. DOI: 10.1016/j.cej.2020.127707

Fernandez, M. E., Ledesma, B., Román, S., Bonelli, P. R., and Cukierman, A. L. (2015). "Development and characterization of activated hydrochars from orange peels as potential adsorbents for emerging organic contaminants," *Bioresource Technol*. 183, 221-228. DOI: 10.1016/j.biortech.2015.02.035

González, D., Colón, J., Gabriel, D., and Sánchez, A. (2019). "The effect of the composting time on the gaseous emissions and the compost stability in a full-scale sewage sludge composting plant," *Sci. Total Environ*. 654, 311-323. DOI: 10.1016/j.scitotenv.2018.11.081

Hameed, B. H., Ahmad, A. A., and Aziz, N. (2007). "Isotherms, kinetics and thermodynamics of acid dye adsorption on activated palm ash," *Chem. Eng. J*. 133, 195-203. DOI: 10.1016/j.cej.2007.01.032

Hubbe, M. A., Azizian, S., and Douven, S. (2019). "Implications of apparent pseudo-second-order adsorption kinetics onto cellulosic materials: A review," *BioResources* 14(3), 7582-7626. DOI: 10.15376/biores.14.3.7582-7626

Jayawardhana, Y., Keerthanan, S., Lam, S. S., and Vithanage, M. (2021). "Ethylbenzene and toluene interactions with biochar from municipal solid waste in single and dual systems," *Environ. Res*. 197: 111102-111113. DOI: 10.1016/j.envres.2021.111102

Kim, J. Y., Oh, S., and Park, Y. K. (2020). "Overview of biochar production from preservative-treated wood with detailed analysis of biochar characteristics, heavy metals behaviors, and their ecotoxicity," *J. Hazard Mater*. 364, 121356-121368. DOI: 10.1016/j.jhazmat.2019.121356

Liu, L., Li, Y., and Fan, S. S. (2019). "Preparation of KOH and H_3PO_4 modified biochar and its application in methylene blue removal from aqueous solution," *Processes* 7, 891-910. DOI: 10.3390/pr7120891

Liu, M. L., Liu, C. J., Liao, W. H., Xie, J. Z., Zhang, X. X., and Gao, Z. L. (2021). "Impact of biochar application on gas emissions from liquid pig manure storage," *Sci. Total Environ*. 771, 145454-145463. DOI: 10.1016/j.scitotenv.2021.145454

Maulini-Duran, C., Artola, A., Font, X., and Sánchez, A. (2013). "A systematic study of the gaseous emissions from biosolids composting: Raw sludge versus anaerobically digested sludge. *Bioresource Technol.* 147, 43-51. DOI: 10.1016/j.biortech.2013.07.118

Rajabi, H., Mosleh, M. H., Prakoso, T., Ghaemi, N., Mandal, P., Lea-Langton, A., and Sedighi, M. (2021). "Competitive adsorption of multicomponent volatile organic compounds on biochar," *Chemosphere* 283, 131288-131296. DOI: 10.1016/j.chemosphere.2021.131288

Seo, J. Y., Tokmurzin, D., Lee, D., Lee, S. H., Seo, M. W., and Park, Y. K. (2022). "Production of biochar from crop residues and its application for biofuel production processes – An overview," *Bioresource Technol.* 361, 127740-127752. DOI: 10.1016/j.biortech.2022.127740

Shen, Y. F., and Zhang, N. Y. (2019). "Facile synthesis of porous carbons from silica-rich rice husk char for volatile organic compounds (VOCs) sorption," *Bioresource Technol.* 282, 294-300. DOI: 10.1016/j.biortech.2019.03.025

Sun, K., Huang, Q. X., Ali, M., Chi, Y., and Yan, J. H. (2018). "Producing aromatic-enriched oil from mixed plastics using activated biochar as catalyst," *Energy Fuels* 32, 5471-5479. DOI: 10.1021/acs.energyfuels.7b03710

Wang, B. D., Gan, F. L., Dai, Z. D., Ma, S. G., Chen, W. H., and Jiang, X. (2021). "Air oxidation coupling NH_3 treatment of biomass derived hierarchical porous biochar for enhanced toluene removal," *J. Hazard Mater*. 403, 123995-124003. DOI: 10.1016/j.jhazmat.2020.123995

Wang, K., Du, M. F., Wang, Z., Liu, H. M., Zhao, Y., Wu, C. D., and Tian, Y. (2022a). "Effects of bulking agents on greenhouse gases and related genes in sludge composting," *Bioresource Technol.* 344, 126270-126278. DOI: 10.1016/j.biortech.2021.126270

Wang, P. P., Cao, J. L., Mao, L. G., Zhu, L. Z., Zhang, Y. N., Zhang, L., Jiang, H. Y., Zheng, Y. Q., and Liu, X. G. (2022b). "Effect of H_3PO_4-modified biochar on the fate of atrazine and remediation of bacterial community in atrazine-contaminated soil," *Sci. Total Environ*. 851, 158278-158287. DOI: 10.1016/j.scitotenv.2022.158278

Wysocka, I., Gębicki, J., and Namieśnik, J. (2019). "Technologies for deodorization of malodorous gases," *Environ. Sci. Pollut. Res. Int.* 26, 9409-9434. DOI: 10.1007/s11356-019-04195-1

Yue, X. C., Ma, N. L., Sonne, C., Guan, R. R., Lam, S. S., Le, Q. V., Chen, X. M., Yang, Y. F., Gu, H.P., Rinklebe, J., and Peng, W. X. (2021). "Mitigation of indoor air pollution: A review of recent advances in adsorption materials and catalytic oxidation," *J. Hazard. Mater*. 405, 124138-124150. DOI: 10.1016/j.jhazmat.2020.124138

Zeng, X. Y., Wang, Y., Li, R. X., Cao, H. L., Li, Y. F., and Lü, J. (2022). "Impacts of temperatures and phosphoric-acid modification to the physicochemical properties of biochar for excellent sulfadiazine adsorption," *Biochar* 4, 14-27. DOI: 10.1007/s42773-022-00143-4

Zhang, X. Y., Gao, B., Zheng, Y. L., Hu, X., Creamer, A. E., Annable, M. D., and Li, Y. C. (2017). "Biochar for volatile organic compound (VOC) removal: Sorption performance and governing mechanisms," *Bioresource Technol.* 245, 606-614. DOI: 10.1016/j.biortech.2017.09.025

Zhang, Y. F., Xiao, J. F., Zhang, T. C., Ouyang, L., and Yuan, S. J. (2022). "Synthesis of $CuSiO_3$-loaded P-doped porous biochar derived from phytic acid-activated lemon peel for enhanced adsorption of NH_3," *Sep. Purif. Technol*. 283, 120179-120190. DOI: 10.1016/j.seppur.2021.120179

Zhao, Z., Wang, B., Theng, B. K. G., Lee, X. Q., Zhang, X. Y., Chen, M., and Xu, P. (2022a). "Removal performance, mechanisms, and influencing factors of biochar for air pollutants: A critical review," *Biochar* 4, 30-53. DOI:10.1007/s42773-022-00156-z

Zhao, Y. X., Lou, Y. C., Qin, W. Z., Cai, J. J., Zhang, P., and Hu, B. L. (2022b). "Interval aeration improves degradation and humification by enhancing microbial interactions in the composting process," *Bioresource Technol.* 358: 127296-127304. DOI: 10.1016/j.biortech.2022.127296

Zheng, G. R., Liu, C. G., Deng, Z., Wei, Z. M., Zhao, Y., Qi, H. S., Xie, X. Y., Wu, D., Zhang, Z. C., and Yang, H. Y. (2021). "Identifying the role of exogenous amino acids in catalyzing lignocellulosic biomass into humus during straw composting," *Bioresource Technol.* 340, 125639-125644. DOI: 10.1016/j.biortech.2021.125639

Zhu, X. M., Yang, X. F., Gao, W., Jiao, R. Y., Zhao, S., Yu, J. W., and Wang, D. S. (2022). "Effect of low-temperature thermal drying on malodorous volatile organic compounds (MVOCs) emission of wastewater sludge: The relationship with microbial communities," *Environ Pollut*. 306, 119423-119431. DOI: 10.1016/j.envpol.2022.119423